PHYSICAL REVIEW C **93**, 044605 (2016)

Asymptotic and near-target direct breakup of ^{6}Li and ^{7}Li

Sunil Kalkal,[*] E. C. Simpson, D. H. Luong, K. J. Cook, M. Dasgupta, D. J. Hinde, I. P. Carter, D. Y. Jeung, G. Mohanto,
C. S. Palshetkar, E. Prasad, D. C. Rafferty, C. Simenel, K. Vo-Phuoc, and E. Williams
Department of Nuclear Physics, Research School of Physics and Engineering, Australian National University, Canberra, ACT 2601, Australia

L. R. Gasques
Instituto de Física, Universidade de São Paulo, São Paulo 05315-970, Brazil

P. R. S. Gomes and R. Linares
Instituto de Física, Universidade Federal Fluminense, Avenida Litoranea s/n, Gragoatá, Niterói, Rio de Janeiro 24210-340, Brazil

(Received 25 February 2016; published 8 April 2016)

Background: ^{6,7}Li and ^{9}Be are weakly bound against breakup into their cluster constituents. Breakup location is important for determining the role of breakup in above-barrier complete fusion suppression. Recent works have pointed out that experimental observables can be used to separate near-target and asymptotic breakup.
Purpose: Our purpose is to distinguish near-target and asymptotic direct breakup of ^{6,7}Li in reactions with nuclei in different mass regions.
Method: Charged particle coincidence measurements are carried out with pulsed ^{6,7}Li beams on ^{58}Ni and ^{64}Zn targets at sub-barrier energies and compared with previous measurements using ^{208}Pb and ^{209}Bi targets. A detector array providing a large angular coverage is used, along with time-of-flight information to give definitive particle identification of the direct breakup fragments.
Results: In interactions of ^{6}Li with ^{58}Ni and ^{64}Zn, direct breakup occurs only asymptotically far away from the target. However, in interactions with ^{208}Pb and ^{209}Bi, near-target breakup occurs in addition to asymptotic breakup. Direct breakup of ^{7}Li into α-t is not observed in interactions with ^{58}Ni and ^{64}Zn. However, near-target dominated direct breakup was observed in measurements with ^{208}Pb and ^{209}Bi. A modified version of the Monte Carlo classical trajectory model code PLATYPUS, which explicitly takes into account lifetimes associated with unbound states, is used to simulate sub-barrier breakup reactions.
Conclusions: Near-target breakup in interactions with ^{6,7}Li is an important mechanism only for the heavy targets ^{208}Pb and ^{209}Bi. There is insignificant near-target direct breakup of ^{6}Li and no direct breakup of ^{7}Li in reactions with ^{58}Ni and ^{64}Zn. Therefore, direct breakup is unlikely to suppress the above-barrier fusion cross section in reactions of ^{6,7}Li with ^{58}Ni and ^{64}Zn nuclei.

DOI: 10.1103/PhysRevC.93.044605

I. INTRODUCTION

Collisions involving weakly bound stable and unstable nuclei are interesting from the perspective of understanding both nuclear structure and nuclear reactions. Information has been obtained on clusters in nuclei [1–3], the effect of breakup on other reaction observables [4–17], and nuclear structure near drip lines [18,19]. In astrophysics, direct Coulomb breakup has been used to probe radiative capture reactions at low energies [20–23]. Here, our interest lies in the effect of breakup on fusion cross sections.

Breakup prior to reaching the fusion barrier is thought to be one reason for the observed ~30% suppression of above-barrier complete fusion cross sections for reactions of ^{6,7}Li and ^{9}Be with heavy target nuclei [4–7,24–26]. Such a suppression is not observed [24,26] in reactions with well-bound nuclei (where breakup should be negligible) forming the same compound system. A smaller suppression of complete fusion has been reported in measurements for reactions of ^{6}Li with ^{64}Ni [27], ^{96}Zr [9], and ^{9}Be with ^{89}Y [28]. Complete fusion measurements are, however, sparse for light and medium-mass nuclei, since separation of complete and incomplete fusion products is difficult. This is because charged particle evaporation from a light compound nucleus is much more significant than that in heavier nuclei. The same reaction product can thus be formed by charged particle evaporation after complete fusion and by incomplete fusion, where only part of the charge of the projectile is captured. For this reason, the extracted complete and incomplete fusion cross sections are often reliant on estimates of charged particle evaporation probabilities from statistical models. This has precluded a systematic understanding of complete fusion suppression from fusion measurements alone, as well as the relationship between above-barrier complete fusion suppression and breakup.

An alternate approach towards this goal has been developed in recent years [29–31], in which breakup mechanisms are studied in detail at sub-barrier energies [7,32]. The charged fragment absorption leading to incomplete fusion is minimal at sub-barrier energies, thus allowing a clearer understanding to be developed. Coincident measurements of charged particles resulting from breakup of the projectile-like nucleus, measured at a range of sub-barrier energies and angles, allows determination of breakup probabilities as a function of the

---

[*] sunil.kalkal@anu.edu.au

distance of closest approach. This "breakup function" is then used as an input to the classical trajectory model PLATYPUS [32–34], which is used to predict above-barrier complete and incomplete fusion cross sections [29], thus providing a link between breakup at sub-barrier energies and above-barrier complete and incomplete fusion.

Recent experimental investigations of breakup have clearly demonstrated that in reactions of the weakly bound nuclei ^{6,7}Li and ^{9}Be, breakup can occur both by direct excitation of projectiles into continuum states (including narrow resonances) and by population of unbound states of a projectile-like nucleus following nucleon transfer [29,30]. Irrespective of the breakup mode, the location of breakup is crucial to above-barrier fusion suppression [30]. Complete fusion can only be suppressed if breakup of the projectile-like nucleus occurs while approaching the target nucleus, before passing inside the fusion barrier radius. At subbarrier energies, the equivalent condition is when breakup occurs as the two nuclei approach each other. Whether this condition is satisfied depends on two factors: (a) the location of the process that triggers breakup and (b) the lifetime of the populated unbound state. Depending on the lifetime of the state populated, the decay (breakup) location can range from close to the target-like nucleus to asymptotically far from the target-like nucleus. If breakup occurs close to the target-like nucleus, the angular and energy correlations of the charged breakup fragments are modified by the Coulomb field of the target-like nucleus [30], whereas the correlations between fragments resulting from breakup occurring asymptotically far from the target-like nucleus are influenced only by their own mutual Coulomb field. Therefore, coincident measurements of energy and angular correlations of breakup fragments provide a means to investigate the locations of breakup [35].

In this paper, we report on an investigation of the direct breakup of ^{6,7}Li incident on targets of ^{58}Ni, ^{64}Zn, and ^{207,208}Pb and ^{209}Bi [30,31] at sub-barrier energies. The targets were chosen in order to investigate the dependence of near-target and asymptotic direct breakup on the strength of the Coulomb interaction between colliding nuclei. The paper is organized as follows: experimental details and data analysis are described in Sec. II; different approaches to separating near-target breakup from asymptotic breakup are discussed in Sec. III; details of the classical dynamical code used for simulations are presented in Sec. IV; experimental results are compared with simulations in Sec. V; and results are summarized and conclusions presented in Sec. VI.

II. EXPERIMENTAL DETAILS AND DATA ANALYSIS

The experiment was performed at the Australian National University (ANU) using the Heavy Ion Accelerator Facility. Pulsed ^{6,7}Li beams (width ~ 1 ns; separation ~ 106.6 ns) were provided by the 14UD tandem accelerator and bombarded thin targets of isotopically enriched ^{58}Ni and ^{64}Zn. The target thicknesses together with the beam energies and the Coulomb barrier for these systems (calculated using the São Paulo potential [36]) are listed in Table I. The ^{58}Ni target was self-supporting, whereas the ^{64}Zn target had a carbon backing 10 μg/cm^2 thick, mounted such that the carbon backing faced the beam. The targets were mounted at 45° to the beam direction such that the plane of the target faced the detectors.

TABLE I. Beam-target combinations, target thicknesses, beam energies (E_{lab}), fusion barriers in the center-of-mass frame (V_b) calculated using the São Paulo potential, and ratios of center-of-mass beam energy ($E_{\mathrm{c.m.}}$) to fusion barrier energy. Beam energies have been corrected for energy loss through half the target thickness and the carbon backing (for ^{64}Zn).

Beam	Target	Thickness (μg/cm^2)	E_{lab} (MeV)	V_b (MeV)	$E_{\mathrm{c.m.}}/V_b$
^{6}Li	^{58}Ni	50	13.07	12.36	0.96
^{6}Li	^{64}Zn	100	13.55	13.05	0.95
^{7}Li	^{58}Ni	50	13.07	12.14	0.96
^{7}Li	^{64}Zn	100	13.60	12.83	0.95

The energy, position, and time of flight (TOF) of the charged breakup fragments were measured in coincidence using the Breakup Array for Light Nuclei (BALiN). This array consists of four double-sided silicon strip detectors (DSSDs), each 400 μm thick, and divided into 16 arcs and 8 sectors, giving a total of 512 effective position pixels across the array. For the measurements with ^{58}Ni and ^{64}Zn targets, the DSSDs were placed in a "front-back" geometry, with two detectors placed in the forward hemisphere and two in the backward hemisphere, as shown in Fig. 1. A 0.7-μm-thick Mylar foil was placed in front of each DSSD to stop electrons. The plane of each detector is at an apex angle of 45° to the beam axis. Figure 2(a) shows the distribution of coincident breakup events seen in the array as a function of the scattering angle (θ) and azimuthal angle (ϕ). The two backward DSSDs covered 101° to 165° in θ and 184° to 330° in ϕ. The most forward angles of the two forward DSSDs were shielded to avoid a high elastic count rate, resulting in an angular coverage of 55° to 84.5° in θ and 32° to

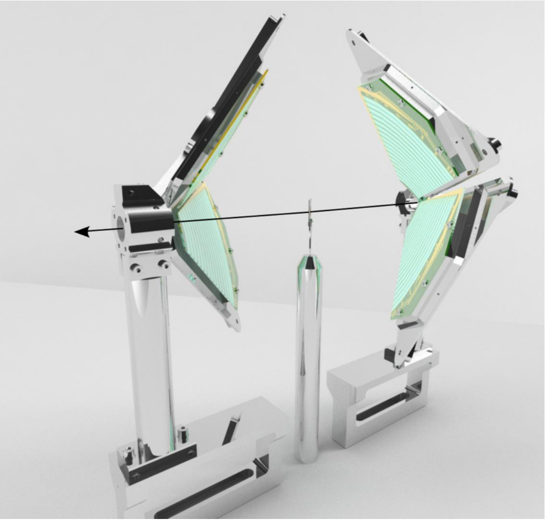

FIG. 1. The BALiN array as configured for the present measurements in the "front-back" geometry. The arrow indicates the beam direction. The two detectors mounted at forward angles were placed at backward angles in the previous measurements for ^{6,7}Li $+^{207,208}$Pb and ^{209}Bi, forming a "lampshade" configuration.

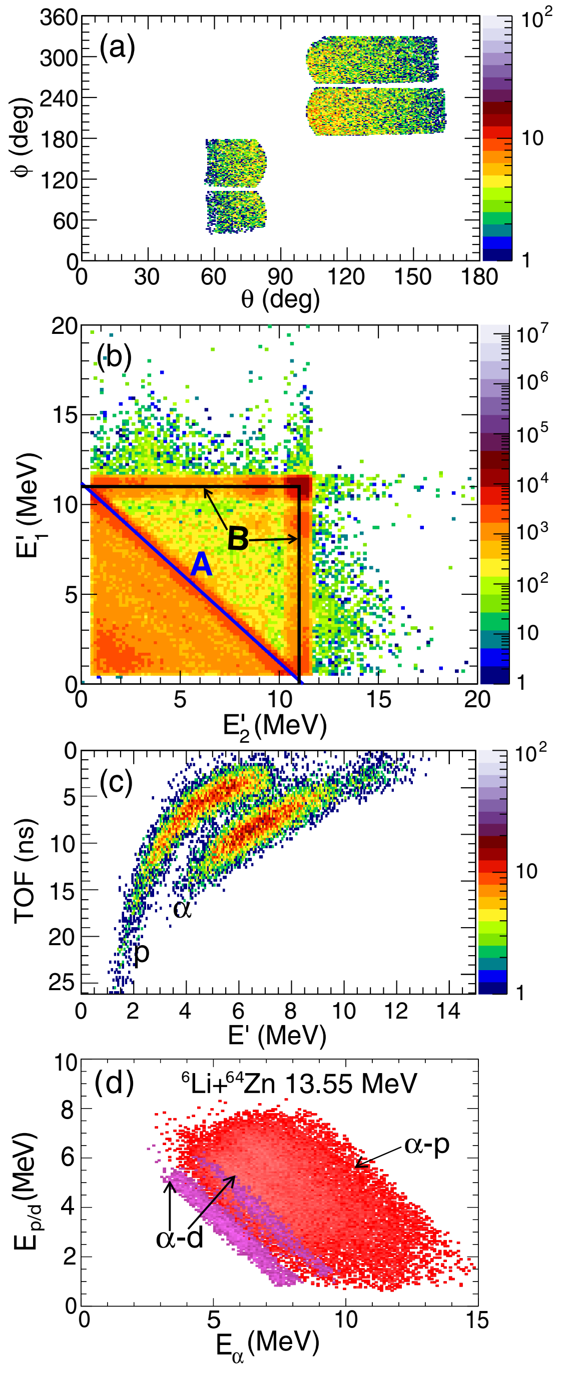

FIG. 2. Two-dimensional spectra of breakup pairs for ^{6}Li + ^{64}Zn at 13.55 MeV. (a) Hit pattern of the coincident breakup events, which is indicative of the detector coverage (in θ,ϕ); (b) uncorrected arc energies (see text) of two coincident fragments, E'_1 and E'_2; (c) time-of-flight (TOF) vs energy (E') of the fragments; (d) corrected energies of the fragment pairs identified as α-p (red) and α-d (purple) as described in the text. Paler shades indicate higher counts per pixel.

178° in ϕ. Two monitor detectors were mounted at ±50° for beam monitoring and normalization to enable the extraction of the breakup cross sections. The measurements for the ^{207,208}Pb and ^{209}Bi targets were carried out previously at the ANU and are described in Ref. [31]. In these measurements, the BALiN array was arranged in a "lampshade" geometry, with DSSDs placed in the backward hemisphere and monitor detectors at ±22.5°.

Energy calibration for each arc and sector was performed using a mixed (^{239}Pu, ^{241}Am, and ^{244}Cm) α source and a measurement of elastically scattered ^{7}Li from ^{144}Sm at a beam energy of 9.70 MeV. At this energy, elastic scattering is pure Rutherford even at the most backward angles of the array. Thus, the elastic yields measured by the monitor detectors and in each pixel in the BALiN array were used to obtain the solid angle ratio of the two monitor detectors to that of each pixel.

A. Removal of elastic false coincidences

The measured arc energies E'_1 and E'_2 of coincident particles from reactions of ^{6}Li with ^{64}Zn at 13.55 MeV energy are shown in Fig. 2(b). These energies are uncorrected for energy losses through half the target thickness, the Mylar foil, and the dead layers of the DSSDs. These corrections can only be carried out after particle identification. At this stage, the assignment of particles to E'_1 or E'_2 is random. Events corresponding to elastic cross-talk between adjacent arcs, where the sum of E'_1 and E'_2 is approximately equal to the energy of elastically scattered ^{6}Li, lie on the intense diagonal band labeled "A" in the figure. These events are generated when elastically scattered beam particles hit the boundary between two arcs, and charge is collected on both arcs, generating signals in adjacent arcs. Similar events are generated when elastically scattered beam particles hit the boundary between two sectors. Random coincidences between elastically scattered ^{6}Li and other particles appear as intense horizontal and vertical bands labeled "B." The elastic cross-talk in arcs and sectors and random coincidence events are removed during off-line data analysis by (i) removing events registered in adjacent pixels with a summed energy equal to that expected for elastic scattering and (ii) applying a narrow gate in energy as a function of the scattering angle to reject events where one particle is an elastically scattered beam.

B. Identification of breakup modes

In the off-line analysis, corrections for energy losses in the dead layers of the DSSDs, the Mylar foil, and the target are performed event by event for all possible charged particles generated from breakup. Once the breakup modes are identified via the subsequent analysis described below, the energy losses appropriate for the identified fragments are then assigned. It is assumed that the point of interaction is at the target center. Since the exact interaction location of particles within each detector pixel cannot be known, the positions of events are randomized within each pixel. This defines the angular resolution of typically $\delta\theta \sim \pm 2^\circ$ for these measurements. For the measurements of ^{6,7}Li reactions with ^{58}Ni and ^{64}Zn, the $Q_{\rm val}$ vs $E_{\rm rel}$ spectrum and TOF vs E' spectrum [shown in Fig. 2(c)] are used to identify the breakup modes [e.g., the two modes illustrated in 2(d)], as described in Secs. II B 1 and II B 2. For the ^{6,7}Li + ^{207,208}Pb and ^{209}Bi systems, breakup modes are identified using $Q_{\rm val}$ vs $E_{\rm rel}$, and particle identification is achieved using the $\Delta E - E$ technique, as described in Refs. [30,31].

1. Q_{val} vs E_{rel}

The fragment energies E_1 and E_2, corrected for energy losses, and the measured θ and ϕ are used to reconstruct key reaction observables such as the Q value (Q_{val}) and relative energy between the two fragments (E_{rel}). The Q_{val} for each breakup mode is reconstructed from the deduced E_1 and E_2 using energy conservation:

$$Q_{\mathrm{val}} = E_1 + E_2 + E_{\mathrm{rec}} - E_{\mathrm{lab}}. \tag{1}$$

Here E_{lab} is the beam energy corrected for energy losses in half of the target thickness and the carbon backing (in ^{64}Zn). The energy of the recoiling nucleus E_{rec} is reconstructed using momentum conservation in three body kinematics. If the assumption of three-body kinematics and the assigned breakup mode is correct, then the Q-value spectrum is expected to show sharp peaks corresponding to states of the recoiling target-like nucleus. Information about the state of the projectile-like nucleus cannot be obtained from the reconstructed Q_{val} since the excitation energy prior to breakup appears in E_1 and E_2. However, useful information about the projectile excitation and location of breakup is carried by the relative energy E_{rel} of the fragments [29,30]:

$$E_{\mathrm{rel}} = \frac{m_1 E_2 + m_2 E_1 - 2\sqrt{m_1 E_1 m_2 E_2}\cos\theta_{12}}{m_1 + m_2}. \tag{2}$$

Here, m_1 and m_2 are the deduced masses of the breakup fragments and θ_{12} their opening angles. In the present measurements, events arising from breakup of ^{6,7}Li in interactions with nuclei of the backing, or target impurities, such as carbon or oxygen, can be removed by performing the kinematic reconstruction assuming the target to be carbon or oxygen. This resulted in sharp peaks at the appropriate Q values, confirming their origin. These events are then removed by gating them out using their Q_{val} vs E_{rel} histograms. Having removed events from these impurities, the individual breakup modes from interactions with the intended target material are identified based on Q_{val} vs E_{rel} spectra. The final Q_{val} vs E_{rel} spectra for breakup following collisions of ^{7}Li with ^{209}Bi and ^{64}Zn are shown in Figs. 3(b) and 3(d), respectively, and the projected Q_{val} spectra are presented in Figs. 3(a) and 3(c), respectively. The identified breakup modes are indicated. Details of identifying the different breakup modes with the ^{209}Bi target can be found in Ref. [31].

For measurements with ^{64}Zn, there was no significant yield at the expected position for α-t breakup indicated by the dashed blue line. Thus, it could not be separated from α-d and α-p (when the reaction leads to excited states of a target-like nucleus giving $Q_{\mathrm{val}} < 2.0$ MeV) as shown in Figs. 3(c) and 3(d). In any case, all these events (indicated in gray) contribute less than 1% of the total breakup yield. For the ^{7}Li + ^{64}Zn reaction, the distributions of α-α and α-p breakup events show considerable overlap in the Q_{val} as well as in the Q_{val} vs E_{rel} spectrum, as shown in Figs. 3(c) and 3(d), respectively. Separation is possible only by using TOF information, as discussed below. The TOF is also used to achieve the correct association of energy and mass of essentially all breakup fragments. The correct energy-mass assignment allows appropriate energy loss corrections and results in the sharp peaks in the reconstructed E_{rel} and Q_{val} spectra [shown in Fig. 3(d)].

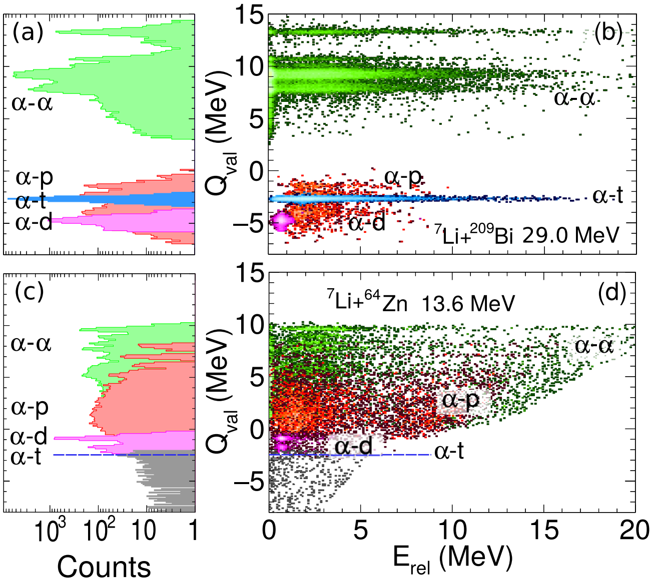

FIG. 3. Q_{val} vs E_{rel} spectra of breakup pairs for ^{7}Li + ^{209}Bi, ^{64}Zn are shown in (b) and (d), and their Q-value distributions are shown in (a) and (c) respectively. α-α breakup events are shown in green; α-p in red, α-d in magenta, and α-t in blue. For ^{7}Li + ^{64}Zn, a clear peak at the position expected for α-t breakup (indicated by dashed blue lines) is not seen in the experiment. See text for details.

2. Time of flight

To extract TOF information for each particle, fast timing signals were obtained from each arc of the detector, and times were determined using leading-edge discriminators. TOF was defined with respect to the radio-frequency signal associated with the time of arrival of the beam pulses. Since the distance from the target to each pixel in the BALiN array was different, the resulting TOF spectrum varied from pixel to pixel. Further, there was a constant offset between the TOF spectra resulting from each arc timing signal being processed individually. By normalizing the TOF of the elastically scattered peak in each detector pixel with respect to a reference pixel during off-line analysis, both of these effects were removed.

The short flight paths, 8–11 cm, result in small differences in flight time between protons and deuterons and between deuterons and tritons. Although protons, deuterons, and α particles could not be identified uniquely, the α particles could be separated from protons and deuterons in the TOF vs E' spectrum alone. This allowed the combination of Q_{val} vs E_{rel} with TOF vs E' to generally provide clear identification of the fragments and the breakup modes. For example, the α-d and α-t modes can be separated from the α-α and α-p modes based on the differences in the Q_{val} vs E_{rel} spectrum. On the other hand, α-α and α-p modes have overlapping Q_{val} vs E_{rel} but are well separated in TOF vs E'. This is illustrated in Fig. 2(c), which has been produced with a requirement of $Q_{\mathrm{val}} > -1.5$ MeV to exclude α-d and α-t breakup modes. Thus, the only particles present should be p and α. The separation between α particles and protons is larger than the difference in flight times over the 8- to 11-cm flight paths. Differences in pulse rise times, in conjunction with leading-edge timing, enhance the separation.

Following the procedure described above that allowed the clear identification of the breakup modes, the rest of the paper focuses exclusively on the direct breakup of ^{6}Li into α-d and ^{7}Li into α-t. In that context, it is interesting to revisit the E_1' vs E_2' plot shown in Fig. 2(b) and extract events corresponding to particular breakup modes, which are shown in Fig. 2(d). The two distinct bands in the direct breakup of ^{6}Li into α-d correspond to coincident events when both charged breakup fragments are detected either in the front detectors or in the back detectors. The separate bands arise because of the different target recoil energies under these two conditions; excited states in the target-like nucleus were not populated. In the case of α-p breakup, separate bands are not evident since events resulting from front-back coincidences are significant, and a number of excited states of the target-like nucleus are populated. Both factors lead to a continuous distribution in the target recoil energy and thus a continuous distribution in E_p vs E_α. The reconstruction of the energy of the recoiling target-like nucleus from momentum conservation is essential to obtain the correct Q value. The resulting sharp peaks in the Q_{val} spectrum [shown in Fig. 3(c)] confirm the correct assignment of the breakup fragment identity.

III. CHARACTERIZING BREAKUP

To relate subbarrier breakup measurements to above-barrier incomplete fusion and to understand the role of breakup in complete fusion suppression, it is necessary to separate near-target breakup from that which occurs asymptotically far from the target nucleus. In recent works [29,31], this information has been obtained from the E_{rel} distribution of the two coincident fragments. In this section, the limitations of characterizing breakup based on E_{rel} are discussed, and the application of a new method [35] for the separation of near-target breakup from asymptotic breakup using angular correlations of breakup fragments is demonstrated.

A. E_{rel}: Near-target vs asymptotic

The basic premise of separation using E_{rel} is that post-breakup acceleration of the charged breakup fragments depends on their proximity to the target [30]. If breakup occurs asymptotically far from the target-like nucleus, then the observed E_{rel} will be equal to the sum of the Q value of the breakup and the excitation energy of the resonant state from which breakup occurs. However, if breakup occurs close to the target, as would be expected for breakup of short-lived states, then the Coulomb interaction between the target and breakup fragments will result in a distorted and smoothed E_{rel} distribution [30,31]. An example of this is shown in Fig. 4(a) for α-d breakup of ^{6}Li with various targets at $E/V_b = 0.95$. The sharp peak at 0.71 MeV (shown by the dashed line) corresponds to direct breakup of ^{6}Li from the long-lived 3^+ resonant state (with a mean life of 2.7×10^{-20} s) [37]. The rest of the events without any characteristic structure should be due to breakup occurring near the target. The E_{rel} distribution extends to 4–5 MeV in reactions with the ^{58}Ni and ^{64}Zn targets, whereas for the ^{207,208}Pb and ^{209}Bi targets it extends to ∼15 MeV, reflecting the stronger Coulomb interaction with these heavy target nuclei. To exclude the possibility of the different detector geometry affecting the conclusions, E_{rel} distributions in reactions with ^{64}Zn are shown in Fig. 4(a) for the two detector geometries: front-back and lampshade. A difference is seen only at higher E_{rel} values, which arises due to the different coincidence detection efficiencies for these two geometries.

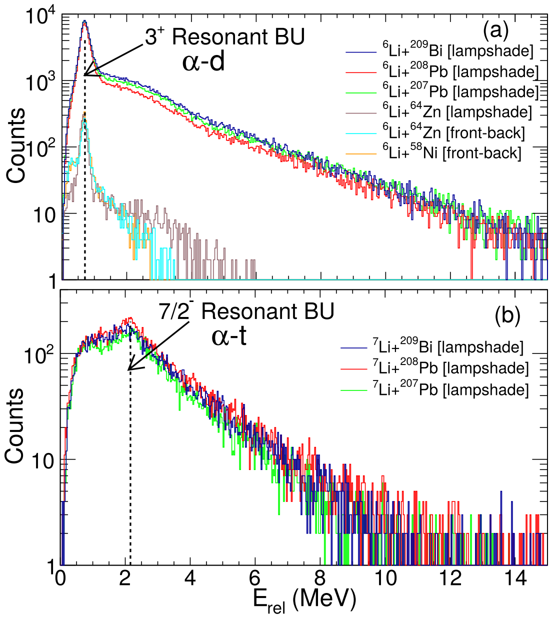

FIG. 4. Direct breakup E_{rel} spectra (a) for α-d breakup pairs for $^6\mathrm{Li} + {}^{58}$Ni, ^{64}Zn, ^{207,208}Pb, and ^{209}Bi reactions and (b) for α-t breakup pairs for $^7\mathrm{Li} + {}^{207,208}$Pb and ^{209}Bi reactions. Dashed vertical lines indicate the expected E_{rel} from breakup of the long-lived 3^+ resonant state in ^{6}Li and from breakup of the long-lived $7/2^-$ resonant state in ^{7}Li.

Shown in Fig. 4(b) are the E_{rel} distributions for α-t breakup of ^{7}Li in reactions with ^{207,208}Pb and ^{209}Bi at 29.0 MeV beam energy. From this figure, it is not possible to clearly separate breakup from the long-lived 4.65 MeV $7/2^-$ resonance state of ^{7}Li (width = 69 keV; mean life = 9×10^{-21} s) [37] from near-target breakup, as there is just a hint of a peak at the expected value in E_{rel}. There were no α-t breakup events clearly identified with the ^{58}Ni and ^{64}Zn targets, as discussed in Sec. II.

B. β vs θ_{12}: Near-target vs asymptotic

Breakup from long-lived resonant states can be separated more cleanly from near-target breakup using angular correlations between the breakup fragments. It has recently been shown [35] that a useful quantity is the orientation of the relative velocity of the fragments with respect to the motion of

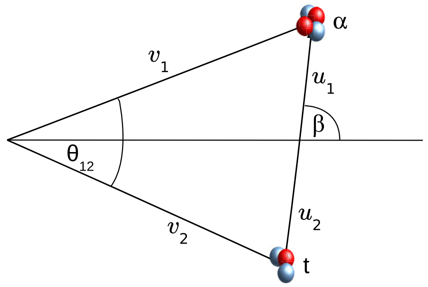

FIG. 5. Schematic showing the relationships between various variables used in Eq. (3) for breakup into α-t.

their center of mass. This angle β is determined from

$$\sin\beta = \frac{v_1 v_2 \sin\theta_{12}}{\left(v_2^2 u_1^2 + v_1^2 u_2^2 + 2u_1 u_2 v_1 v_2 \cos\theta_{12}\right)^{1/2}}, \qquad (3)$$

where v_i and u_i are the particle velocities in the laboratory and composite rest frames, respectively. A schematic showing the relationships between all these variables is shown in Fig. 5.

Plotted against the opening angle θ_{12}, the β distribution yields information about the location of breakup relative to the target-like nucleus [35]. In simulations as well as experimental data, particle 1 is the heavier and 2 is the lighter. The expected correlation between β and θ_{12} for asymptotic breakup [obtained from Eq. (3)] from the 3^+ resonant state of ^{6}Li and the $7/2^-$ resonant state of ^{7}Li is shown by dashed lines in Figs. 6(a) and 6(b), respectively. Figure 6(a) shows a distinct correlation between β and θ_{12} for breakup events from the long-lived 3^+ resonance state in ^{6}Li following the turquoise dashed line, as the fragments are not affected by the presence of the target Coulomb field. The same is true for breakup occurring from the long-lived $7/2^-$ resonance state in ^{7}Li (dashed black line), enabling much clearer identification of these events as shown in Fig. 6(b). This was less obvious using the $E_{\rm rel}$ distribution as noted previously. The excellent agreement of this correlation assuming asymptotic breakup using Eq. (3) for the long-lived resonant states of ^{6,7}Li with the experimental data illustrates that this correlation can be measured accurately.

For events arising from breakup of ^{6,7}Li near the target, the β vs θ_{12} correlation will be distorted due to post-breakup Coulomb acceleration of the breakup fragments as discussed below and in Ref. [35]. Therefore, this correlation gives a handle on the location of the breakup. This observable has the advantage that one can better distinguish near-target and asymptotic breakup, particularly if one is weaker than the other. In the next section, classical dynamical simulations of the breakup under different assumptions regarding the proximity to the target are presented and discussed.

IV. MODELING PROMPT AND ASYMPTOTIC BREAKUP

In order to better understand the near-target breakup component we make simulations of breakup using a classical three-body dynamical model, PLATYPUS [32–34]. It simulates the trajectories of fragments following breakup of the projectile. The trajectory of the projectile and target is tracked up to some point where the projectile is selected to break up into two fragments. The locations of breakup are stochastically sampled assuming that the probability of breakup increases exponentially with decreasing distance between the projectile and the target. As such, the reaction positions are concentrated near the distance of closest approach on the projectile and target trajectory. The original version of PLATYPUS allowed for a uniform or exponentially decaying projectile nucleus excitation energy distribution within given energy limits. In the modified version, the initial relative energy of the fragments—equivalent to the excitation of ^{6,7}Li*—is randomly sampled from a given input distribution. The target and two breakup fragments are then propagated in time, with their mutual interactions defined by Coulomb and nuclear Woods-Saxon potentials. Here we make several other modifications to PLATYPUS [34] to give an improved—though still phenomenological—description of the breakup process.

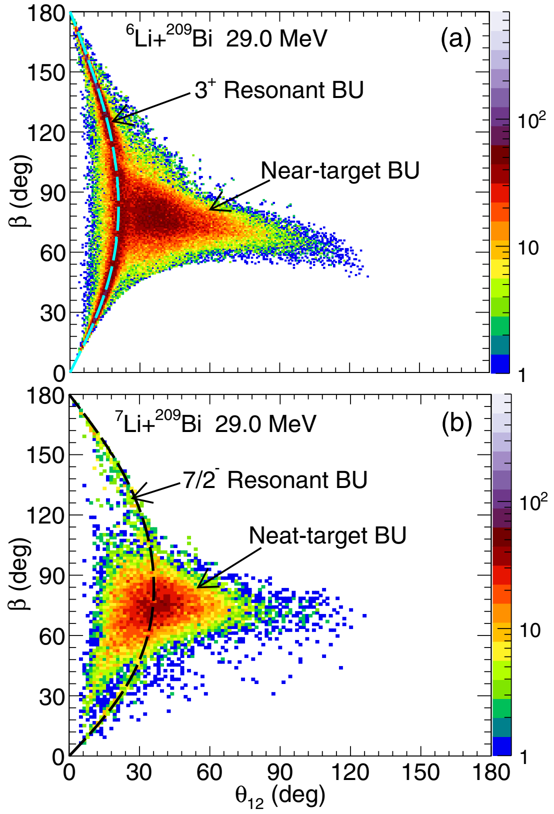

FIG. 6. The β vs θ_{12} spectra of breakup pairs for ^{6,7}Li + ^{209}Bi at 29.0 MeV. Dashed lines show the expected β vs θ_{12} correlation assuming asymptotic breakup from the long-lived 3^+ resonant state in ^{6}Li and $7/2^-$ resonant state in ^{7}Li.

A. Modifications to the breakup function

Breakup probabilities are found experimentally to depend exponentially on the distance of closest approach $R_{\rm min}$ (see, e.g., [7,32]). In PLATYPUS the integrated probability of breakup on a given trajectory is fixed by $R_{\rm min}$. The local breakup probability $\mathcal{P}_{\rm BU}(R)$ is a function of the projectile-target separation R, with $\mathcal{P}_{\rm BU}(R)dR$ giving the probability of breakup between

R and $R + dR$:

$$P_{\mathrm{BU}}(R_{\min}) = 2\int_{R_{\min}}^{\infty} \mathcal{P}_{\mathrm{BU}}(R)dR = A\exp(-\alpha R_{\min}). \quad (4)$$

From the above it is assumed that the local probability function has the same exponential form, $\mathcal{P}_{\mathrm{BU}}(R) \propto \exp(-\alpha R)$. The exponential form means that the local breakup function P_{BU} is naturally peaked at the distance of closest approach $R_{\min}$. However, it is at the turning point that the radial separation changes most slowly, and the probability associated with the radial interval dR spreads over an increasingly long time interval as $R_{\min}$ is approached. The implied breakup probability for time steps near the turning point then becomes small.

Instead, for each time step on the projectile-target trajectory we evaluate the local breakup probability $\mathcal{P}_{\mathrm{BU}}(R)$. These probabilities are then renormalized such that their sum matches that of the input breakup function. This ensures that the breakup is peaked near the distance of closest approach. The importance of this change is, however, case dependent. The negative reaction Q value for the direct breakup discussed here means that there is a classically forbidden region near the turning point. In practice, then, this change only has a small effect for negative Q-value reactions but may be important for transfer reactions with positive Q-values.

B. Lifetimes prior to breakup

In PLATYPUS, it is assumed that breakup is instantaneous. The instant the excitation of the projectile is chosen to occur, the projectile is immediately converted into its cluster constituents ($^6\mathrm{Li} \to \alpha$-d, $^7\mathrm{Li} \to \alpha$-t), and the fragments and the target then propagate according to their defined mutual interactions. The initial separation of the two fragments (α-d, α-t) is stochastically sampled from a Gaussian distribution, the size of which is chosen to simulate the projectile ground state.

This approach has a number of implications for the model. The two fragments may remain spatially localized for some period after the reaction has occurred, as it will take some finite time for them to reach their mutual barrier and move irreversibly apart. This represents an effective lifetime. However, this effective lifetime is sensitive to the excitation of the state (i.e., the initial relative energy of the fragments), the relative angular momentum of the fragments, and the depth of the potential chosen to simulate their mutual interaction. Tidal forces generated by the target nucleus may also influence how long the fragments remain localized.

However, it is evident from analysis of experimental E_{rel} distributions and β vs θ_{12} correlations that breakup can occur both near the target and asymptotically far away. The lifetimes of the states in $^6\mathrm{Li}^*$ or $^7\mathrm{Li}^*$, for which the two fragments remain strongly spatially correlated, are therefore important. Here, we have modified the simulation to allow us to explicitly specify this lifetime. As before, the reaction point is stochastically sampled, and the trajectories of the target and composite (e.g., $^{6,7}\mathrm{Li}^*$) determined. A lifetime for the composite is then randomly determined based on the input mean life, which may be given as a function of the excitation energy of the composite state. The system (target plus composite) is then propagated for the duration of the lifetime. Once this intermediate propagation has occurred, the breakup fragments (α-d, α-t) are created with a separation equal to the peak of their relative barrier or, for low excitation, the outer turning point of their potential. The fragments then propagate radially away from one another.

This approach neglects tidal forces for the duration of the intermediate propagation of $^{6,7}\mathrm{Li}^*$. In effect, one can envisage the fragments propagating outwards with respect to one another, with no influence of the target on their relative motion until they pass their mutual barrier. The impact of tidal forces within the classical model is not obvious. Depending on the orientation of the fragments with respect to the target, and their respective charge-to-mass ratios, the tidal forces could shorten or prolong the period of spatial localization. However, the approach taken here allows for an explicit and well-defined distribution of mean life (discussed in the next section) to be used and avoids the sensitivity to the fragment-fragment potential.

C. Asymptotic breakup

The experimental data for direct breakup of both ^{6}Li and ^{7}Li show evidence of long-lived, narrow resonances at low excitation energies. For ^{6}Li, the 3^+ state at 2.186 MeV is strongly populated. The state has a width $\Gamma = 24$ keV, corresponding to a mean life of 27 zs. The $7/2^-$ state in ^{7}Li, as shown in Fig. 6(b), is weakly populated but has a similar width, $\Gamma = 69$ keV, and a mean life of 9 zs. The mean lives of both states are long enough that they will, in general, decay into fragments only when they have receded from the target. The cluster constituents remain spatially localized until they have moved sufficiently far from the target, and the subsequent interaction with the target will have little effect on their relative motion. To describe this within the model we need to estimate (a) the relative probability, $\rho_\ell(E)$, of populating the excitation energy E above the relevant threshold, in the composite nucleus ($^{6,7}\mathrm{Li}^*$), and (b) the mean life corresponding to this E.

For well-defined narrow resonances, the expected distribution $\rho_\ell(E)$ can be estimated in the one-state, one-channel limit of R-matrix theory [38,39]:

$$\rho_\ell(E) \propto \frac{\Gamma_\ell(E)}{[E_R + \Delta_\ell(E) - E]^2 + \left[\frac{1}{2}\Gamma_\ell(E)\right]^2}. \quad (5)$$

Here $\Gamma_\ell(E)$ is the energy-dependent resonance width and $\Delta_\ell(E) = S(E) - B$, where $S(E)$ is the shift function [40], and B an constant boundary condition parameter. B is set to the shift function at the resonance energy $S(E_R)$, resulting in $\Delta_\ell(E_R) = 0$. The width $\Gamma_\ell(E)$ can be written in terms of the underlying reduced-width amplitude

$$\Gamma_\ell(E) = 2P_\ell(E)\gamma_\ell^2, \quad (6)$$

where $P_\ell(E)$ is the penetrability calculated from regular and irregular Coulomb wave functions at radius R_n, which depends on the relative angular momentum ℓ of the two fragments [40]. The radius parameter R_n differentiates the internal (pure nuclear) and external (pure Coulomb) regions. γ_ℓ is the reduced width amplitude and, in R-matrix models, is related to the overlap integral of the internal compound nucleus state with the external outgoing wave functions, over the dividing surface defined by R_n. We choose the reduced-width amplitude γ_ℓ

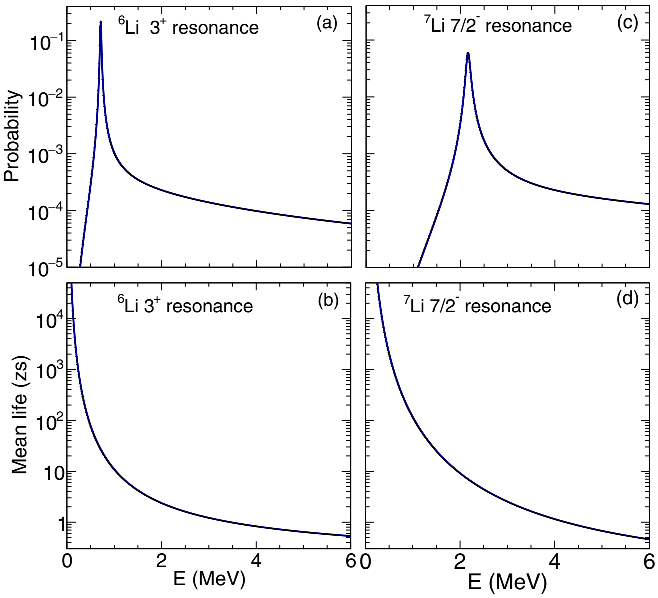

FIG. 7. (a) Probability of populating the excitation energies (E) above the breakup threshold for 3^+ resonant states of ^{6}Li used in simulations. (b) Excitation energy dependent mean life for (a). (c) Same as (a) for $7/2^-$ resonant states of ^{7}Li used in simulations. (d) Excitation energy dependent mean life for (c).

to match the experimentally observed on-resonance width $\Gamma_\ell(E_R)$ [41]. Using this γ_ℓ, $\rho_l(E)$ may then be calculated for all excitation energies, and the corresponding mean life is estimated using $\tau(E) = \hbar/\Gamma_l(E)$. Given this assumed form for the excitation distribution and corresponding life, the forms used for the resonant states in ^{6}Li and ^{7}Li are shown in Fig. 7.

D. Near-target breakup

In addition to the narrow resonances identified in both ^{6}Li and ^{7}Li, a broad background is also observed as shown in Figs. 4 and 6. The origin of this component is not clear. Both ^{6}Li and ^{7}Li have additional broad resonances at higher energies than the narrow states observed, which could be populated in the interaction with the target. Also, the breakup could populate short-lived nonresonant continuum states. Alternatively, tidal forces generated by the target could cause the narrow resonant states to break up faster than would otherwise be expected. Regardless of the source, it is assumed that this component results from near-target breakup, with the subsequent post-breakup acceleration of the fragments significantly changing their relative energy, obscuring potential signatures of the source.

Given this ambiguity in the mechanism for near-target breakup, we assume that the near-target breakup occurs quickly and take the upper limit for the width, giving a lower limit for the mean life as discussed below. The reduced-width amplitude is assumed to be equal to the Wigner limit (pure single-particle state; see Refs. [40,42–44]) giving an upper limit for the width [44],

$$\Gamma_\ell(E) = 2P_\ell(E)\frac{\hbar^2}{\mu R_n^2}. \tag{7}$$

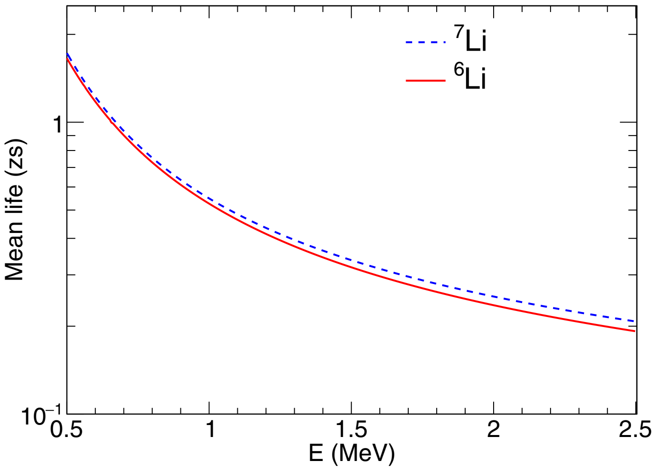

FIG. 8. Excitation energy (E) dependent mean life of the short-lived states (which break up near the target) of ^{6,7}Li. Excitation energies are with regard to the breakup threshold of these nuclei. The solid red line represents ^{6}Li; the dashed blue line ^{7}Li.

The corresponding (lower-limit) mean life is again given by $\tau(E) = \hbar/\Gamma_\ell(E)$. Here we choose $\ell = 0$, giving the minimum expected mean life. Since the mechanism for near-target breakup is not clear, we assume a uniform probability for exciting ^{6,7}Li* between 0.5 and 2.5 MeV above the threshold. The estimated mean lives for ^{6}Li and ^{7}Li nonresonant states are shown in Fig. 8. The long mean life of the nonresonant component is attributed to its low energy and low probability of penetrating the mutual barrier of the fragments (α-d, α-t).

Earlier applications of this approach [22,23,45,46] focused on Coulomb dissociation of ^{7}Li, producing α-t coincidences at the low relative energy of less than 1 MeV. Resulting from the population of ^{7}Li at energies just above the threshold, these events show little evidence of post-breakup Coulomb acceleration.

V. RESULTS AND DISCUSSION

In this section, the experimentally measured $E_{\rm rel}$ and β vs θ_{12} spectra are compared with the new classical simulations which explicitly include the distributions of excitation energies and the mean lives associated with these states as described in the previous section. The results of the simulations shown here are filtered through the experimental detector geometry and the angles of the fragments are randomized within each pixel as done for the experimental data. Thus the effect of detector pixelation on reconstructed quantities is identical in the experimental data and simulations. As PLATYPUS allows breakup reactions to be tracked in detail, a comparison with experimental measurements can be used to provide information about positions of breakup and the effect of the mean life associated with unbound states. In the subsequent subsections, the experimental results of direct breakup of ^{6,7}Li are compared with the simulations for targets in different mass regions.

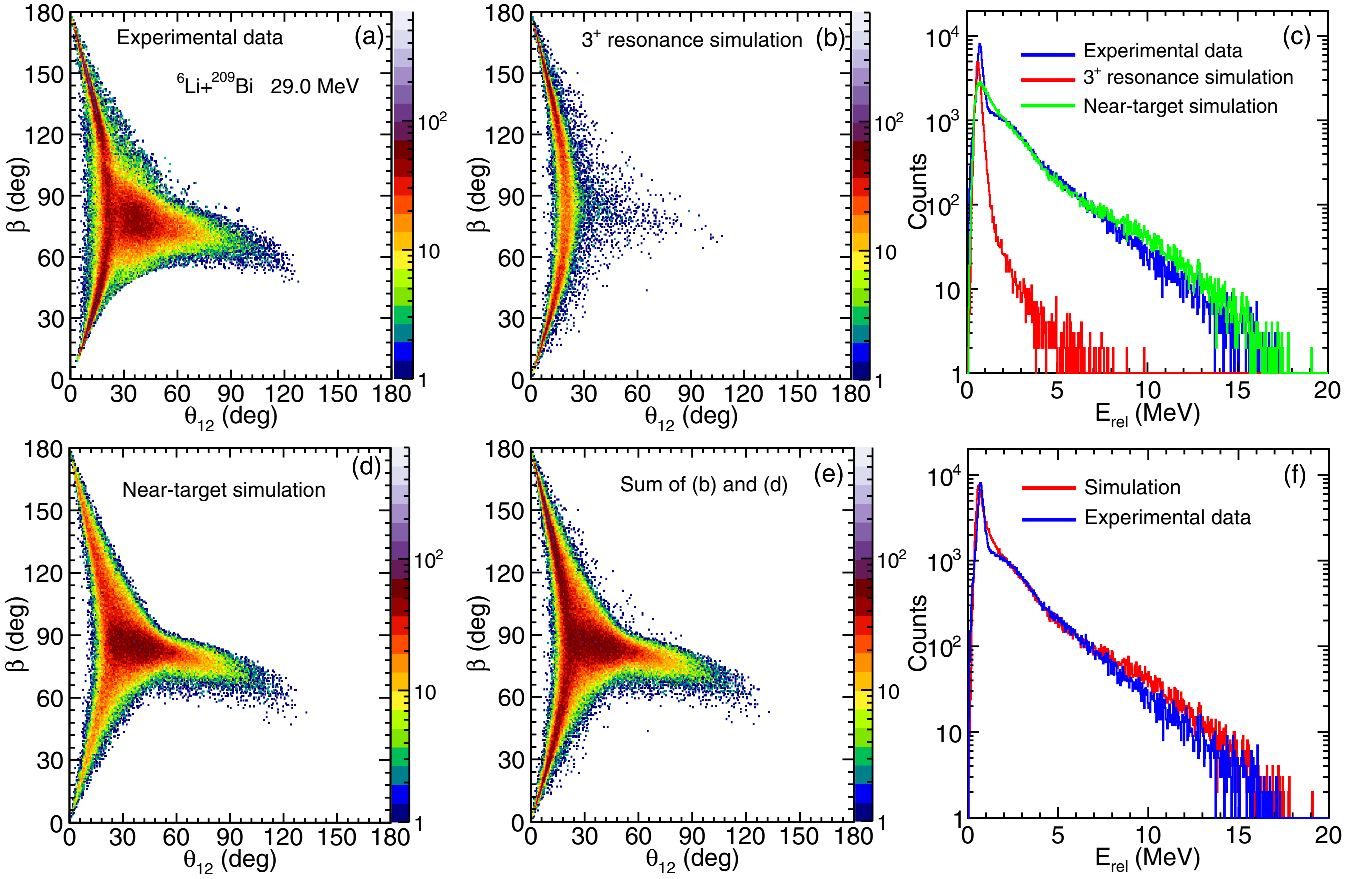

FIG. 9. Experimental data and simulations for ^{6}Li breakup into α-d in reactions with ^{209}Bi at 29.0 MeV beam energy. (a) Experimental β vs θ_{12} distribution; (b) simulation of breakup occurring from the long-lived 3^+ resonant state in ^{6}Li; (c) experimental E_{rel} distribution (blue), PLATYPUS simulations assuming breakup from the 3^+ resonance (red), and PLATYPUS simulations assuming breakup from the short-lived states (green); (d) PLATYPUS simulations for breakup occurring from short-lived states of ^{6}Li; (e) sum of simulations in (b) and (d); (f) experimental E_{rel} distribution (blue) and PLATYPUS simulations (red) for (e).

A. Direct breakup of ^{6}Li in collisions with ^{209}Bi

The experimental β vs θ_{12} distribution is shown in Fig. 9(a) for ^{6}Li direct breakup into α-d in collisions with ^{209}Bi target nuclei. Figure 9(b) shows the β vs θ_{12} distribution obtained from a PLATYPUS simulation of breakup occurring only through the long-lived resonant 3^+ state, while Fig. 9(c) shows a comparison of the E_{rel} distribution obtained from this simulation (red line) vs experimental data (blue line). The simulation of breakup from the 3^+ resonant state fails to reproduce a large component of the experimental data [Fig. 9(a)] at high θ_{12} and E_{rel}. These events must, therefore, have a different origin. Their distributions of E_{rel} and β vs θ_{12} can be reproduced reasonably well by simulations of breakup of ^{6}Li from short-lived states with mean lives from the red solid line given in Fig. 8. These results are shown in Figs. 9(c) and 9(d), respectively. The simulations of breakup of ^{6}Li from the 3^+ resonant state and short-lived states (filtered by the BALiN detection efficiency) are merged to reproduce the experimental data reasonably well, as shown in Figs. 9(e) and 9(f). The unfiltered events comprised 26% of the total direct breakup events originating from the 3^+ resonant state and 74% from the short-lived states. This indicates that the direct breakup of ^{6}Li occurs through both long-lived resonant and short-lived states in interactions with heavy target nuclei such as ^{209}Bi. Very similar E_{rel} [as shown in Fig. 4(a)] and β vs θ_{12} distributions were observed in interactions of ^{6}Li with ^{207,208}Pb.

B. Direct breakup of ^{6}Li in collisions with ^{58}Ni and ^{64}Zn

The classical simulations for breakup from the long-lived 3^+ resonance in ^{6}Li reproduce the experimental distributions of β vs θ_{12} for the ^{64}Zn target reasonably well as shown by comparing Figs. 10(a) and 10(b). The width of the peak in the E_{rel} distribution is also well reproduced for the long-lived resonant state as shown in Fig. 10(c). For ease of comparison, simulations are shown with a similar number of events as the experimental data. There is an excess of events in the experimental β vs θ_{12} spectrum at $\beta \sim 90^\circ$ and large θ_{12} over that seen in the simulation, which may be due to breakup close to the target. These events having higher θ_{12} constitute less than 7% of the total events. The fact that the experimental data are well reproduced by simulation from the long-lived 3^+ resonant state alone indicates that breakup proceeds mainly via the 3^+ resonant state. A similar kind of agreement is obtained for the direct breakup of ^{6}Li in reactions with ^{58}Ni.

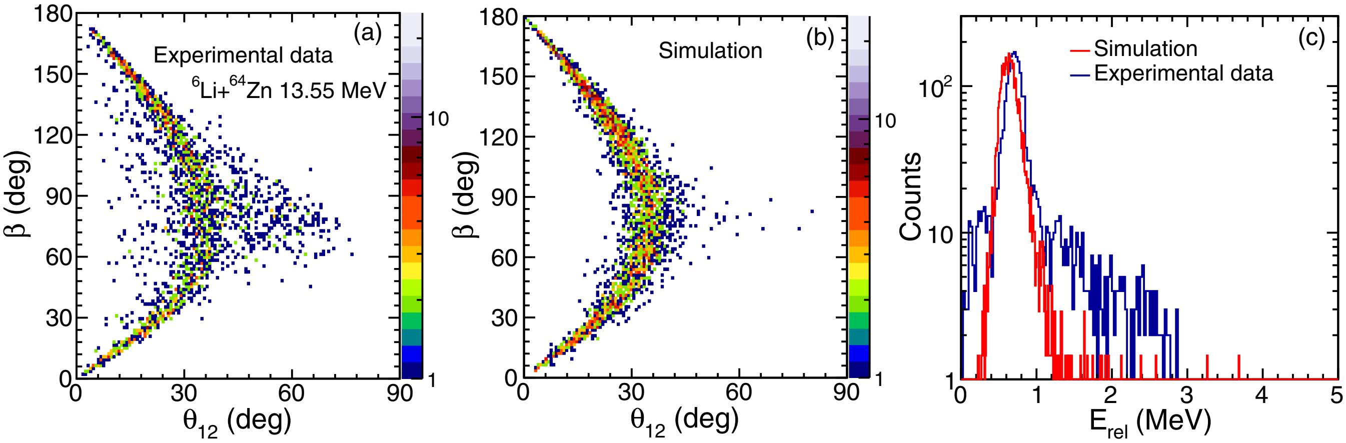

FIG. 10. Comparison of experimental data with simulation for ^{6}Li incident on the ^{64}Zn target at 13.55 MeV. (a) Experimental β vs θ_{12} distribution; (b) simulations for ^{6}Li breaking into α-d from the 3^+ resonant state; and (c) comparison of experimental (blue) and simulated (red) $E_{\rm rel}$ distribution.

C. Direct breakup of ^{7}Li in collisions with ^{209}Bi

The experimental β vs θ_{12} and $E_{\rm rel}$ distributions along with classical simulations for the direct breakup of ^{7}Li after interactions with ^{209}Bi target are shown in Fig. 11. The experimental distribution is shown in Fig. 11(a). In Figs. 11(b) and 11(c), simulations for the long-lived $7/2^-$ resonant state and short-lived continuum states (filtered by the BALiN detection efficiency) are merged to reproduce the experimental data. The unfiltered events comprised 7% of the total direct breakup events originating from the long-lived $7/2^-$ resonant state and 93% from short-lived states. The simulations reproduce the qualitative features of the experimental data. In the experimental data, there are no events corresponding to $\beta \geqslant 115^\circ$ and θ_{12} values lower than the $7/2^-$ band, whereas simulations show a significant number of events in this region. This results in a peak in the simulated $E_{\rm rel}$ distribution [shown in Fig. 11(c)] at $E_{\rm rel} < 1$ MeV. Experimental data with $\beta \geqslant 115^\circ$ are clearly identified from the decay of the long-lived $7/2^-$ resonant state in ^{7}Li as shown in Fig. 11(a). There are events detected at the same values of β and θ_{12} in the direct breakup of ^{6}Li in interactions with the same target as shown in Fig. 9(a). Thus, the absence of the experimental data on near-target direct breakup of ^{7}Li in this region is not due to any experimental limitation. These subtle differences indicate that the β vs θ_{12} distribution carries detailed information about the locations of breakup and the model needs further refinement.

D. Direct breakup of ^{7}Li in collisions with ^{58}Ni and ^{64}Zn

As shown in Fig. 3(b), direct breakup events in reactions of ^{7}Li with ^{209}Bi are clearly observed at $Q_{\rm val} = -2.47$ MeV, which corresponds to the Q value for the breakup of ^{7}Li into α-t. Direct breakup of ^{7}Li is also seen in reactions with ^{207,208}Pb as shown in Fig. 4(b). However, no such clear band is observed for reactions with ^{64}Zn as shown in Fig. 3(d) and discussed in Sec. II. Likewise, there was no identifiable peak at the expected Q value for the direct breakup of ^{7}Li with the ^{58}Ni target. The absence of the direct breakup mode with ^{58}Ni and

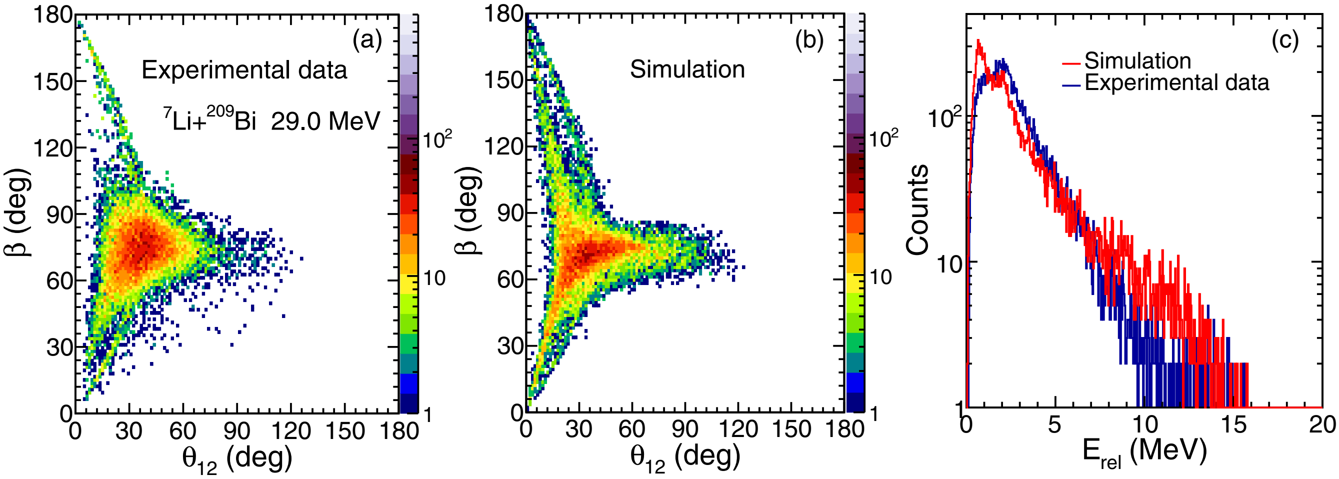

FIG. 11. Comparison of experimental data (a) and (c) with simulations (b) and (c) for ^{7}Li on ^{209}Bi at 29.0 MeV. The simulations comprise breakup occurring from the long-lived $7/2^-$ resonant state and short-lived states. See text for details.

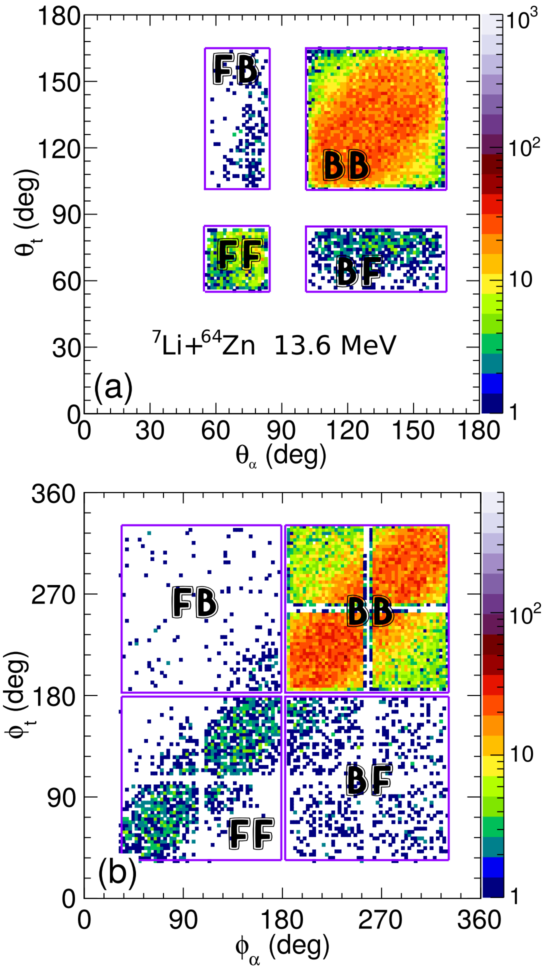

FIG. 12. Simulation of direct breakup of ^{7}Li into α-t with ^{64}Zn at 13.6 MeV. The θ_t vs θ_α and ϕ_t vs ϕ_α distributions of events that would have been detected for breakup of ^{7}Li occurring near the target are shown in (a) and (b), respectively. BB: both fragments are expected to be in the backward hemisphere. FF: both are expected to be in the forward hemisphere. FB and BF: the α is expected to be in the forward hemisphere and the triton in the backward hemisphere, and vice versa.

^{64}Zn is not because of the limitation in detector coverage. This is supported by PLATYPUS simulations of direct breakup of ^{7}Li from short-lived states in interactions with a ^{64}Zn target. The angular correlation of the breakup fragments within the BALiN geometrical and energy acceptance for ^{7}Li on a ^{64}Zn target at 13.6 MeV is shown in Fig. 12. The rectangular regions in Figs. 12(a) and 12(b) indicate the θ and ϕ distribution of events within the angular acceptance of the BALiN array. It shows clearly that α-t coincident events would have been detected and identified if present.

E. Comparison of direct breakup mechanisms of ^{7}Li and ^{6}Li

For extraction of the cross sections, the experimental data need to be corrected for the efficiency of the BALiN array. The efficiency correction is performed by simulating a large number of events using PLATYPUS. The efficiency-corrected fractions for asymptotic and near-target direct breakup in interactions of ^{6,7}Li with ^{64}Zn and ^{209}Bi are listed in Table II. From the table, it is clear that the direct breakup mechanism is very different in interactions with nuclei in different mass regions. In collisions of ^{6}Li with ^{58}Ni and ^{64}Zn, the majority of events arise due to asymptotic breakup from the long-lived 3^+ resonant state. No discernible direct breakup of ^{7}Li is observed with ^{58}Ni and ^{64}Zn.

TABLE II. Asymptotic and near-target direct breakup of ^{6,7}Li in interactions with ^{64}Zn and ^{209}Bi at $E_{\mathrm{c.m.}}/V_b = 0.95$ as a fraction of the total number of efficiency-corrected events.

	^{6}Li		^{7}Li	
	Asymptotic	Near-target	Asymptotic	Near-target
^{64}Zn	0.93[a]	0.07[a]	None observed	
^{209}Bi	0.26	0.74	0.07	0.93

[a] Assuming the same detection efficiency.

In reactions of ^{6}Li with ^{209}Bi, as listed in Table II, the near-target direct breakup is the dominant mode. Similarly to ^{6}Li, the dominant mode of direct breakup of ^{7}Li in interactions with ^{209}Bi is via decay of short-lived states near the target. Since these measurements were performed at subbarrier energies, one would expect that breakup is Coulomb dominated. The steeper Coulomb potential should allow population of higher energies, which have short lifetimes, and also induce more tidal breakup of the long-lived states. Comparing direct breakup of ^{6,7}Li with ^{209}Bi, the long-lived 3^+ resonant state in ^{6}Li is found to be more important than the $7/2^-$ resonance in ^{7}Li. This may be explained by the fact that the 3^+ resonance at 2.186 MeV in ^{6}Li lies 0.711 MeV above the breakup threshold of ^{6}Li ($Q_{\alpha d} = -1.475$ MeV), whereas the $7/2^-$ resonance in ^{7}Li at 4.630 MeV is 2.162 MeV above the ^{7}Li breakup threshold ($Q_{\alpha t} = -2.468$ MeV). These differences lead to very different probabilities of populating short-lived states relative to the lowest energy resonant state in these two nuclei. The fractions of asymptotic and near-target direct breakup of ^{6,7}Li in reactions with ^{207,208}Pb are similar to those in reactions with ^{209}Bi.

The fact that there is negligible near-target direct breakup of ^{6,7}Li in reactions with ^{58}Ni and ^{64}Zn is a major difference compared to reactions with ^{207,208}Pb and ^{209}Bi. Therefore, direct breakup is unlikely to result in suppression of above-barrier fusion in reactions with ^{58}Ni and ^{64}Zn. On the other hand, near-target breakup is dominant for ^{6,7}Li in interactions with ^{207,208}Pb and ^{209}Bi, which may lead to above-barrier fusion suppression. Therefore, to quantify these effects, resonant, near-target, and total direct breakup differential cross sections as a function of the reconstructed scattering angle of the ejectile following collisions of ^{6,7}Li with ^{209}Bi target at 29.0 MeV were extracted and are shown in Figs. 13(a) and 13(b), respectively, and reported in the Appendix. The center-of-mass angle of the ejectile ($\theta_{\mathrm{c.m.}}$) was reconstructed using the measured angles of the breakup fragments [31]. For ^{6,7}Li, the cross sections for near-target breakup are higher than for breakup occurring from the long-lived resonant states. Previous measurements [47] of direct breakup cross sections with ^{6}Li projectiles on ^{209}Bi reported the cross sections for resonant breakup to be higher than those for nonresonant continuum breakup. In those measurements, detectors were

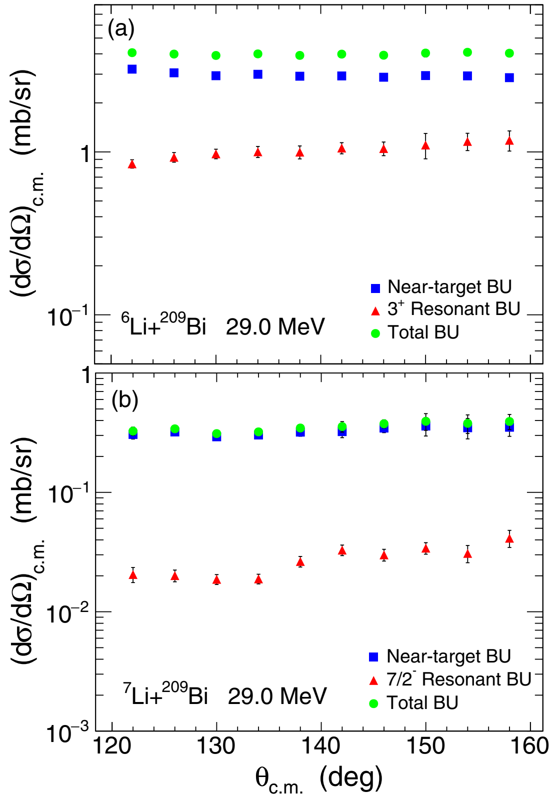

FIG. 13. Differential breakup cross sections vs reconstructed scattering angle of the ejectile ($\theta_{c.m.}$) in the center-of-mass frame for interactions of ^{6,7}Li with ^{209}Bi measured at a beam energy of 29.0 MeV. (a) Resonant, near-target, and total direct breakup with ^{6}Li; (b) same as (a) for breakup of ^{7}Li.

placed at an angular separation of 10°, favoring the detection of asymptotic breakup, as the maximum angle between breakp fragments from decay of the long-lived 3^{+} resonant is expected to be around 16°–19° [48]. The resonant breakup cross sections for ^{6}Li are almost two orders of magnitude larger than those for ^{7}Li and the nonresonant breakup cross sections are also much higher for ^{6}Li compared to ^{7}Li.

VI. SUMMARY AND CONCLUSION

The measurements reported in this paper present a detailed study of direct breakup for weakly bound ^{6,7}Li nuclei incident on targets in different mass regions. An improved method of separating breakup of short-lived states from asymptotic decay of long-lived resonant states is presented. Both ^{6}Li and ^{7}Li in reactions with ^{207,208}Pb and ^{209}Bi show evidence of breakup via a long-lived resonant state, which breaks up asymptotically far away from the target-like nucleus. However, ^{6}Li has a higher probability of direct breakup via the long-lived resonant state than ^{7}Li, which dominantly breaks up via the short-lived states. The near-target direct breakup of ^{6}Li in interactions with ^{58}Ni and ^{64}Zn is observed to be negligible. Direct breakup of ^{7}Li following interactions with ^{58}Ni and ^{64}Zn is insignificant (estimated limit, <0.2 mb). Thus, direct breakup is unlikely to play a significant role in above-barrier fusion suppression in reactions of ^{6,7}Li with ^{58}Ni and ^{64}Zn.

The near-target breakup is consistent with simulations which assume that the continuum states populated have a short but finite mean life, delaying its decay into fragments. At above-barrier energies, if the mean life is long, they may pass inside the fusion barrier by the time they disintegrate. Similar behavior should be expected from breakup occurring from very short-lived states, irrespective of whether the breakup is direct or triggered by transfer of nucleons. In classical model predictions of ICF, it has thus far been assumed that for near-target breakup, there is an equal probability of breakup when the projectile is moving towards the target or when the projectile is receding from the target. This will change if the mean lives associated with the near-target breakup are taken into account, with implications for predicted incomplete fusion cross sections.

APPENDIX: TABLE OF DIRECT BREAKUP DIFFERENTIAL CROSS SECTIONS FOR REACTIONS OF ^{6,7}Li ON ^{209}Bi

The experimental differential cross sections for asymptotic, near-target and total direct break-up of ^{6,7}Li in reactions with ^{209}Bi at 29.0 MeV beam energy are listed in Table III. The corresponding errors are statistical only.

TABLE III. Asymptotic, near-target, and total direct breakup differential cross sections (in mb/sr) of ^{6,7}Li in interactions with a ^{209}Bi target at $E_{\text{lab}} = 29.0$ MeV.

$\theta_{c.m.}$	^{6}Li			^{7}Li		
	Asymptotic	Near-target	Total	Asymptotic	Near-target	Total
122	0.84 ± 0.05	3.22 ± 0.09	4.06 ± 0.10	0.020 ± 0.003	0.31 ± 0.03	0.33 ± 0.03
126	0.93 ± 0.06	3.06 ± 0.08	3.99 ± 0.10	0.020 ± 0.002	0.32 ± 0.02	0.34 ± 0.02
130	0.97 ± 0.06	2.94 ± 0.06	3.91 ± 0.08	0.019 ± 0.002	0.29 ± 0.02	0.31 ± 0.02
134	1.00 ± 0.08	2.99 ± 0.05	3.99 ± 0.09	0.019 ± 0.002	0.30 ± 0.02	0.32 ± 0.02
138	0.99 ± 0.09	2.91 ± 0.07	3.90 ± 0.11	0.026 ± 0.003	0.32 ± 0.02	0.35 ± 0.02
142	1.06 ± 0.08	2.93 ± 0.08	3.99 ± 0.11	0.033 ± 0.003	0.32 ± 0.03	0.35 ± 0.03
146	1.05 ± 0.10	2.87 ± 0.07	3.92 ± 0.12	0.030 ± 0.003	0.34 ± 0.03	0.37 ± 0.03
150	1.10 ± 0.19	2.94 ± 0.08	4.04 ± 0.21	0.034 ± 0.004	0.36 ± 0.06	0.39 ± 0.06
154	1.16 ± 0.14	2.92 ± 0.10	4.08 ± 0.17	0.031 ± 0.005	0.35 ± 0.07	0.38 ± 0.07
158	1.18 ± 0.17	2.86 ± 0.09	4.04 ± 0.19	0.041 ± 0.007	0.35 ± 0.06	0.39 ± 0.06
162	1.07 ± 0.14	2.67 ± 0.08	3.74 ± 0.16	0.037 ± 0.006	0.34 ± 0.07	0.38 ± 0.07

[1] A. H. Wuosmaa, R. R. Betts, M. Freer, and B. R. Fulton, Annu. Rev. Nucl. Part. Sci. **45**, 89 (1995).

[2] T. Yamagata, H. Akimune, S. Nakayama, M. Fujiwara, K. Fushimi, M. B. Greenfield, K. Hara, K. Y. Hara, H. Hashimoto, K. Ichihara *et al.*, Phys. Rev. C **71**, 064316 (2005).

[3] S. Nakayama, T. Yamagata, H. Akimune, M. Fujiwara, K. Fushimi, M. B. Greenfield, K. Hara, K. Y. Hara, H. Hashimoto, K. Ichihara *et al.*, Phys. Rev. C **69**, 041304 (2004).

[4] M. Dasgupta, D. J. Hinde, R. D. Butt, R. M. Anjos, A. C. Berriman, N. Carlin, P. R. S. Gomes, C. R. Morton, J. O. Newton, A. Szanto de Toledo *et al.*, Phys. Rev. Lett. **82**, 1395 (1999).

[5] M. Dasgupta, D. J. Hinde, K. Hagino, S. B. Moraes, P. R. S. Gomes, R. M. Anjos, R. D. Butt, A. C. Berriman, N. Carlin, C. R. Morton *et al.*, Phys. Rev. C **66**, 041602 (2002).

[6] C. L. Guo, G. L. Zhang, S. P. Hu, J. C. Yang, H. Q. Zhang, P. R. S. Gomes, J. Lubian, X. G. Wu, J. Zhong, C. Y. He *et al.*, Phys. Rev. C **92**, 014615 (2015).

[7] D. J. Hinde, M. Dasgupta, B. R. Fulton, C. R. Morton, R. J. Wooliscroft, A. C. Berriman, and K. Hagino, Phys. Rev. Lett. **89**, 272701 (2002).

[8] A. Di Pietro, P. Figuera, E. Strano, M. Fisichella, O. Goryunov, M. Lattuada, C. Maiolino, C. Marchetta, M. Milin, A. Musumarra *et al.*, Phys. Rev. C **87**, 064614 (2013).

[9] S. P. Hu, G. L. Zhang, J. C. Yang, H. Q. Zhang, P. R. S. Gomes, J. Lubian, X. G. Wu, J. Zhong, C. Y. He, Y. Zheng *et al.*, Phys. Rev. C **91**, 044619 (2015).

[10] C. Beck, F. A. Souza, N. Rowley, S. J. Sanders, N. Aissaoui, E. E. Alonso, P. Bednarczyk, N. Carlin, S. Courtin, A. Diaz-Torres *et al.*, Phys. Rev. C **67**, 054602 (2003).

[11] I. Padron, P. R. S. Gomes, R. M. Anjos, J. Lubian, C. Muri, J. J. S. Alves, G. V. Martí, M. Ramírez, A. J. Pacheco, O. A. Capurro *et al.*, Phys. Rev. C **66**, 044608 (2002).

[12] R. M. Anjos, C. Muri, J. Lubian, P. R. S. Gomes, I. Padron, J. J. S. Alves, G. V. Martí, J. O. Fernández Niello, A. J. Pacheco, O. A. Capurro *et al.*, Phys. Lett. B **534**, 45 (2002).

[13] M. Ray, A. Mukherjee, M. K. Pradhan, R. Kshetri, M. S. Sarkar, R. Palit, I. Majumdar, P. K. Joshi, H. C. Jain, and B. Dasmahapatra, Phys. Rev. C **78**, 064617 (2008).

[14] M. Sinha, H. Majumdar, P. Basu, S. Roy, R. Bhattacharya, M. Biswas, M. Pradhan, R. Palit, I. Mazumdar, and S. Kailas, Eur. Phys. J. A **44**, 403 (2010).

[15] A. Diaz-Torres, I. J. Thompson, and C. Beck, Phys. Rev. C **68**, 044607 (2003).

[16] L. F. Canto, P. R. S. Gomes, J. Lubian, L. C. Chamon, and E. Crema, Nucl. Phys. A **821**, 51 (2009).

[17] P. R. S. Gomes, M. D. Rodríguez, G. V. Martí, I. Padron, L. C. Chamon, J. O. Fernández Niello, O. A. Capurro, A. J. Pacheco, J. E. Testoni, A. Arazi *et al.*, Phys. Rev. C **71**, 034608 (2005).

[18] L. Canto, P. R. S. Gomes, R. Donangelo, J. Lubian, and M. Hussein, Phys. Rep. **596**, 1 (2015).

[19] A. García-Camacho, A. Bonaccorso, and D. Brink, Nucl. Phys. A **776**, 118 (2006).

[20] H. Utsunomiya, Y.-W. Lui, D. R. Haenni, H. Dejbakhsh, L. Cooke, B. K. Srivastava, W. Turmel, D. O'Kelly, R. P. Schmitt, D. Shapira *et al.*, Phys. Rev. Lett. **65**, 847 (1990).

[21] G. Baur and H. Rebel, Annu. Rev. Nucl. Part. Sci. **46**, 321 (1996).

[22] H. Utsunomiya, Y. Tokimoto, H. Mabuchi, K. Osada, T. Yamagata, M. Ohta, Y. Aoki, K. Hirota, K. Ieki, Y. Iwata *et al.*, Phys. Lett. B **416**, 43 (1998).

[23] Y. Tokimoto, H. Utsunomiya, T. Yamagata, M. Ohta, Y.-W. Lui, R. P. Schmitt, S. Typel, Y. Aoki, K. Ieki, and K. Katori, Phys. Rev. C **63**, 035801 (2001).

[24] M. Dasgupta, P. R. S. Gomes, D. J. Hinde, S. B. Moraes, R. M. Anjos, A. C. Berriman, R. D. Butt, N. Carlin, J. Lubian, C. R. Morton *et al.*, Phys. Rev. C **70**, 024606 (2004).

[25] C. S. Palshetkar, S. Thakur, V. Nanal, A. Shrivastava, N. Dokania, V. Singh, V. V. Parkar, P. C. Rout, R. Palit, R. G. Pillay *et al.*, Phys. Rev. C **89**, 024607 (2014).

[26] P. K. Rath, S. Santra, N. L. Singh, R. Tripathi, V. V. Parkar, B. K. Nayak, K. Mahata, R. Palit, S. Kumar, S. Mukherjee *et al.*, Phys. Rev. C **79**, 051601 (2009).

[27] M. M. Shaikh, S. Roy, S. Rajbanshi, M. K. Pradhan, A. Mukherjee, P. Basu, S. Pal, V. Nanal, R. G. Pillay, and A. Shrivastava, Phys. Rev. C **90**, 024615 (2014).

[28] C. S. Palshetkar, S. Santra, A. Chatterjee, K. Ramachandran, S. Thakur, S. K. Pandit, K. Mahata, A. Shrivastava, V. V. Parkar, and V. Nanal, Phys. Rev. C **82**, 044608 (2010).

[29] R. Rafiei, R. du Rietz, D. H. Luong, D. J. Hinde, M. Dasgupta, M. Evers, and A. Diaz-Torres, Phys. Rev. C **81**, 024601 (2010).

[30] D. Luong, M. Dasgupta, D. Hinde, R. du Rietz, R. Rafiei, C. J. Lin, M. Evers, and A. Diaz-Torres, Phys. Lett. B **695**, 105 (2011).

[31] D. H. Luong, M. Dasgupta, D. J. Hinde, R. du Rietz, R. Rafiei, C. J. Lin, M. Evers, and A. Diaz-Torres, Phys. Rev. C **88**, 034609 (2013).

[32] A. Diaz-Torres, D. J. Hinde, J. A. Tostevin, M. Dasgupta, and L. R. Gasques, Phys. Rev. Lett. **98**, 152701 (2007).

[33] A. Diaz-Torres, J. Phys. G **37**, 075109 (2010).

[34] A. Diaz-Torres, Comput. Phys. Commun. **182**, 1100 (2011).

[35] E. C. Simpson, K. J. Cook, D. H. Luong, S. Kalkal, I. P. Carter, M. Dasgupta, D. J. Hinde, and E. Williams, Phys. Rev. C **93**, 024605 (2016).

[36] L. C. Chamon, B. V. Carlson, L. R. Gasques, D. Pereira, C. De Conti, M. A. G. Alvarez, M. S. Hussein, M. A. Cândido Ribeiro, E. S. Rossi, and C. P. Silva, Phys. Rev. C **66**, 014610 (2002).

[37] D. R. Tilley, C. M. Cheves, J. L. Godwin, G. M. Hale, H. M. Hofmann, J. H. Kelley, C. G. Sheu, and H. R. Weller, Nucl. Phys. A **708**, 3 (2002).

[38] F. C. Barker, Aust. J. Phys. **41**, 743 (1988).

[39] P. R. Treacy, Philos. Mag. **44**, 325 (1953).

[40] A. M. Lane and R. G. Thomas, Rev. Mod. Phys. **30**, 257 (1958).

[41] F. C. Barker and P. B. Treacy, Nucl. Phys. **38**, 33 (1962).

[42] H. A. Bethe, Rev. Mod. Phys. **9**, 69 (1937).

[43] C. E. Rolfs and W. S. Rodney, *Cauldrons in the Cosmos* (University of Chicago Press, Chicago, 1998), p. 155.

[44] D. D. Clayton, *Principles of Stellar Evolution and Nucleosynthesis*, 2nd ed. (University of Chicago Press, Chicago, 1983), p. 333.

[45] H. Utsunomiya, Y. Tokimoto, K. Osada, T. Yamagata, M. Ohta, Y. Aoki, K. Hirota, K. Ieki, Y. Iwata, K. Katori *et al.*, J. Phys. G **24**, 1637 (1998).

[46] H. Utsunomiya, Y. Tokimoto, K. Osada, T. Yamagata, M. Ohta, Y. Aoki, K. Hirota, K. Ieki, Y. Iwata, K. Katori *et al.*, Nucl. Instrum. Methods Phys. Res. A **402**, 417 (1998).

[47] S. Santra, V. V. Parkar, K. Ramachandran, U. Pal, A. Shrivastava, B. Roy, B. Nayak, A. Chatterjee, R. Choudhury, and S. Kailas, Phys. Lett. B **677**, 139 (2009).

[48] C. Signorini, A. Edifizi, M. Mazzocco, M. Lunardon, D. Fabris, A. Vitturi, P. Scopel, F. Soramel, L. Stroe, G. Prete *et al.*, Phys. Rev. C **67**, 044607 (2003).